Accepted Manuscript

Geological Society, London, Special Publications

Multi-method 2D and 3D reconstruction of gold grains morphology in alluvial deposits: a review and application to the Rivière du Moulin (Québec, Canada)

François-Xavier Masson, Georges Beaudoin & Denis Laurendeau

DOI: https://doi.org/10.1144/SP516-2020-186

To access the most recent version of this article, please click the DOI URL in the line above. When citing this article please include the above DOI.

Received 23 July 2020
Revised 1 March 2021
Accepted 4 March 2021

Multi-method 2D and 3D reconstruction of gold grains morphology in alluvial deposits: a review and application to the Rivière du Moulin (Québec, Canada)

François-Xavier Masson[1,3*], Georges Beaudoin[1,3], Denis Laurendeau[2,3]

1. Université Laval, Département de géologie et de génie géologique, Université Laval, Québec, QC, Canada

2. Université Laval, Département de génie électrique et de génie informatique, Université Laval, Québec, QC, Canada

3. Centre E4m - Centre de Recherche sur la Géologie et l'Ingénierie des Ressources Minérales, Université Laval, Québec, Canada

** Corresponding author: francois-xavier.masson.1@ulaval.ca (Département de géologie et de génie géologique, Université Laval, Pavillon Adrien-Pouliot, 1065, Avenue de la Médecine, Québec, QC, G1V 0A6, Canada).*

Abstract

The aim of this paper is to document and compare the 2D qualitative and semi-quantitative methods currently used to describe the shape of gold grains in fluvial environment to 3D quantitative methods using microtomography and SEM photogrammetry. These 3D methods are used to compute flatness, roundness, convexity, sphericity, and ellipticity shape descriptors of 13 gold grains from the Rivière du Moulin (Québec, Canada) in order to quantify the morphological change along 9 km of fluvial transport. Gold grains have moderate to high values of flatness, compactness, sphericity, and ellipticity indices that do not change significantly with distance of transport, whereas the roundness increases during transport. Gold grains are used to compare 2D and 3D methods and the results show small differences (< 8%) when shape descriptors are computed using image analysis software, whereas the difference (up to 70%) is more important for 2D measurements performed by a human operator. For application and characterization on a large set of gold grains, the 2D methods offer the advantage of speed, whereas, for a more detailed study on a limited number of gold grains, 3D methods enable estimation of the volume and yield more detailed shape descriptors changes during fluvial transport.

Introduction

Native gold is a malleable material of which the shape changes during transport (Hérail et al. 1989; Knight et al. 1999). In mineral exploration, the change in gold grains shape as a function of the distance of transport can help to locate the source of the mineralization (Giusti 1986; Grant et al. 1991; Hérail et al. 1990; Knight et al. 1999; Youngson and Craw 1999; Townley et al. 2003; McClenaghan and Cabri 2011). Visual charts and semi-quantitative approaches are used to estimate a gold grain shape (Hérail et al. 1990; Dilabio 1991; Minter 1999). The general shape, outline, and surface texture have been shown to characterize gold particle morphology (Townley et al. 2003; Craw et al. 2017). In addition to the morphological change, mineral inclusions are commonly used to characterize the source of gold grains in Quaternary sediments (Chapman and Mortensen 2016). Some recent studies use both morphological and geochemical approaches in order to describe the shape evolution during transport from an identified source (Hérail et al. 1990; Youngson et al. 2002; Chapman and Mortensen 2006; Crawford 2007; Wrighton 2013). In this paper, we propose to focus on the morphology of gold grains. The surface texture and gold particle size are transformed after several kilometers (> 5 km) of transport, depending on the abrasion, hammering and folding processes (Knight et al. 1999). The change in shape is studied on gold grains larger than 200 μm, which are more easily collected, and the quantification of a smaller size fraction is not undertaken (Hérail et al. 1989; Knight et al. 1999; Youngson and Craw 1999; Craw et al. 2017). However, in alluvial sediments, an important proportion of gold particles is smaller than 200 μm (e.g. North Saskatchewan and Athabasca rivers, Giusti 1986) and it has been suggested that the particle size decreases as the distance of transport increases (Hérail et al. 1989; Knight et al. 1999; Youngson and Craw 1999; Craw et al. 2017). Thus, the investigation of various particle sizes including the smallest fractions (i.e. < 100-200 μm) would be beneficial for the determination of the morphological change of gold grains during fluvial transport. Three 2D shape descriptors (Table 1) are commonly used to describe the flatness and sphericity of gold grains in the fluvial environment (Knight et al. 1999; Youngson and Craw 1999; Townley et al. 2003; Crawford 2007). In such cases, the volume, surface area and triaxial lengths are used to compute quantitative shape descriptors (Table 1) in 3D (Wadell 1932, 1933; Riley 1941; Aschenbrenner 1956; Hayakawa and Oguchi 2005; Fonseca et al. 2012; Alshibli et al. 2014; Masson 2020). μCT and SEM photogrammetry are two methods used to reconstruct the morphology of gold in

3D (Masson et al. 2020) in order to quantify these 3D shape descriptors for a more complete characteristics of the gold particles.

In this paper, we present a brief review of 2D methods used to estimate the morphology of gold grains. We present the reconstruction of shape and the quantification of 3D shape descriptors to fluvial gold grains (ranging from 42 to 909 μm of long axis) collected in the Rivière du Moulin. This short-distance (9 km) stream is an example of application on a complex Quaternary setting, where the source of gold is unknown and the amount (n = 13) of gold grains analyzed in 3D is limited. Gold grains from the Rivière du Moulin were also measured in 2D to compare shape parameter and descriptor values in order to compare the relative merits of 2D and 3D methodologies for mineral exploration.

Morphology of gold grains in 2D

Estimation of the shape of gold grains in fluvial environment

Gold grains undergo a change in shape and surface texture during transportation as a result of interactions with other sedimentary particles in the stream. The observations of these morphological changes were mainly realized using 2D SEM images (Hérail et al. 1990; Townley et al. 2003; Craw et al. 2017). Some experiments were performed to observe the abrasion effect and the behavior of gold particles in a river bed (Yeend 1975). In the Attappadi Valley (Southern India), placer gold were characterized by differences in the microtextures and corrosion marks (Nakagawa et al. 2005). In the Witwatersrand (South Africa), the distance of transport was estimated between 10 and 30 km, based on visualization of the morphology of gold particles in 2D (Hallbauer and Utter 1977; Utter 1979; Utter 1980). The gold grains show a change from irregular to scratched, abraded, partly rounded, bent, and hammered edges particle with increasing distance of transport (Hallbauer and Utter 1977; Utter 1979; Utter 1980). In Southern and Central Otago (New Zealand), the shape, internal and external surface texture were observed to determine shape modifications of gold particles after transport and deposition (Craw and Lilly 2016; Craw et al. 2017). The minimum and maximum distances were estimated from abrasion marks on the surface of gold grains (Craw et al. 2017). Smear marks indicate fluvial transport of gold particles that have been impacted by sedimentary gravels and document the physical process of the gold grain deformation (Kerr et al. 2017). In the Klondike District (Yukon, Canada), the outline of gold

grains was used to classify gold grain shape in four classes (branched, complex, equant, and elongate) using 2D projections (Knight et al. 1999).

The change of flatness was one of the first shape descriptors used to estimate the distance of transport of gold grains in fluvial environments (Giusti 1986), whereas visual charts (Powers 1953) were used to determine the roundness and sphericity (Eyles 1989). Barrios et al. (2015) developed a new classification of roundness and sphericity of gold grains using visualization and statistical methods in order to improve the chart of Powers (1953). The morphology of gold grains was measured using the length, width, and thickness of the particle in order to compute flatness shape descriptors (Hérail et al. 1990; Barrios et al. 2015). The *Wentworth flatness index* (Wentworth 1922) and the *Corey shape factor* (Corey 1949), are two descriptors commonly used to estimate flatness. An increase in flatness, roundness and sphericity is a typical change in gold grain shape during alluvial transport (Giusti 1986; Hérail et al. 1990; Knight et al. 1999; Youngson and Craw 1999). The *Wentworth flatness index* was used in several studies of gold grain shape in placers (Hérail et al. 1990; Loen 1995; Barrios et al. 2015). In the Tipuani placer (Andes, Bolivia) the *Wentworth flatness index* increases along 70 to 80 km of transport in the river (Hérail et al. 1990). The mean value of the *Wentworth flatness index* close to the source was between 2 and 4 and reached 9 after 30 km, 15 after 60 km, but did not increase after 60 km of transport (Hérail et al. 1990). In Central Otago (New Zealand), the mean value of the *Wentworth flatness index* was 1.8 close to the source and increased to 11.0 and 15.9 at a distance of 75 to 180 km (Youngson and Craw 1999). The *Wentworth flatness index* is constant after a distance of 75 km where forms of folding and refolding gold grains were observed (Youngson and Craw 1999). In the North Saskatchewan and the Athabasca rivers (Alberta, Canada), the *Corey shape factor* was used to quantify flatness of gold particles with respect to their size in order to improve sampling procedures in fluvial environments (Giusti 1986). However, the *Corey shape factor* can be used to estimate a change and increase of flatness during fluvial transport (Barrios et al. 2015). In Witwatersrand, the *Corey shape factor* was estimated on large number of gold grains (over 5,000) and showed an extreme flatness of particles with a mean *Corey shape factor* of 0.08 (Minter et al. 1993).

The Zingg diagram (Zingg 1935) was used to estimate the form (platy, equant, bladed, and elongate) of sedimentary particles with computation of the flatness ratio (short axis/intermediate axis, high for platy particle) and elongate ratio (intermediate axis/long axis, high for elongate particle). This

diagram is used to estimate the shape of the particles based on the triaxial lengths and to determine a shape predominance in a dataset (Wierchowiec 2002). In Witwatersrand, 1,374 gold grains plotted in the Zingg diagram show predominance of oblate (disc-like) shapes for gold grains (Minter et al. 1993). Another shape descriptor, the *Hofmann shape entropy* (Hofmann 1994) was used as a settling velocity or sphericity descriptor (Le Roux 1997), but has been rarely used to describe the shape of gold grains during fluvial transport (Crawford 2007).

Automation of shape quantification

The use of shape descriptors on multiple gold grains is time-consuming such that automation becomes desirable to describe the shape of a large numbers of gold grains (Crawford and Mortensen 2009). The use of image analysis software such as ImageJ (Schneider et al. 2012) enables measurement of the major, intermediate, and minor axis of gold grains (Rasmussen et al. 2006; Crawford 2007; Crawford and Mortensen 2009; Wrighton 2013). The measurements are based on 2D projections of gold grains mounted on adhesive sheets (Crawford 2007; Crawford and Mortensen 2009; Wrighton 2013). This technique enables to compute the *Wentworth flatness index* (Rasmussen et al. 2006; Crawford 2007; Crawford and Mortensen 2009; Wrighton 2013) and the *Hofmann shape entropy* (Crawford 2007; Crawford and Mortensen 2009; Wrighton 2013) on a large number (7,977 in Western Yukon) of gold grains by automated computation (Crawford 2007). The combination of stream dynamics, grain chemistry and morphological analyses enable to constrain more accurately the source of gold and to estimate the distance of transport (Crawford 2007; Wrighton 2013). The computation of a large number of grain shape is important for representative record of morphology (McClenaghan and Cabri 2011). However, sample preparation is time-consuming and the measurement of the minor axis depends on the operator (Crawford and Mortensen 2009), which is a disadvantage of 2D methods such that use of 3D reconstruction of the particle volume may be required (Masson et al. 2020).

Morphometric quantification of gold grains in 3D

Quantification of gold grains with multi-descriptors in 3D

Two methods of analysis can be used to reconstruct the shape of gold grains in 3D. The photogrammetry of scanning electron microscope images (SEM photogrammetry) and the micro-

computed tomography (μCT) were developed to measure axial lengths, surface area and volume (Masson et al. 2020). The reconstruction method of gold grains depends on their size. The μCT method has an optimal resolution to yield full reconstruction of gold grains larger than 85 μm, whereas SEM photogrammetry yields a partial reconstruction for gold grains smaller than 85 μm (Masson et al. 2020). For both methods, gold grains were analyzed individually and placed on the tip of a wood stick coated with a carbon tape to hold them during analysis. A carbon tape is essential to provide a conductive setup for SEM photogrammetry analysis and does not conflict with μCT analysis. The SEM resolution is adequate for small grains (< 85 μm) and secondary-electron images provides surface texture details required for reconstruction by SEM photogrammetry (Masson et al. 2020). Common abrasion marks on the surface of fluvial gold grains are also detected.

Three-dimensional shape descriptors were selected to describe the morphology of gold particle using the dimensions (also measured using 2D methods) and new shape parameters such as surface area, volume, volume of the convex hull, radius of the largest inscribed sphere, and radius the smallest circumscribed sphere derived from 3D reconstruction (Table 1). In addition to these 3D shape descriptors, three common 2D shape descriptors, such as the *Wentworth flatness index* (*FI*), the *Corey shape factor* (*CSF*), and the *Hofmann shape entropy* (*Hr*), were computed in order to estimate a change of gold grains morphology in the Rivière du Moulin (Table 1). 3D shape descriptors are used to quantify non-quantifiable 2D shape descriptors such as roundness, ellipticity, and convexity.

Application to the Rivière du Moulin

Geological setting

The Rivière du Moulin flows over bedrock, till and ancient alluvium cover (Fig. 1). In this area, the basement is composed of shales of the Ordovian Magog Group (Hébert 2001). The Magog Group consists of four formations, but only two of them are present in the study area, the St-Victor and Beauceville formations (Hébert 2001). The St-Victor Formation is composed of turbiditic sequences and felsic volcanoclastic rocks. The Beauceville Formation is mainly composed of graphitic schists as well as felsic volcano-sedimentary rocks and cherts, and hosts most of the hydrothermal gold mineralization north and near the river (Fig. 1). Mineralization occurs in quartz stockwork associated with arsenopyrite

and pyrite hosted in volcano-sedimentary rocks and disseminated gold-bearing pyrite in black shales (Hébert 2001).

A preglacial saprolite layer, enriched in gold, formed in the upper 2 to 5 m of the bedrock (Shilts and Smith 1988; Shilts and Caron 2018). Fourteen gold grains were found in the saprolite in borehole drilled at Rivière Gilbert north of the transect (Shilts and Smith 1988). Weathering contributed to the gold enrichment of the saprolite, which hosts coarse, folded, and rounded grains with pitted surface (Shilts and Smith 1988). However, initial shape of gold grains in the mineralization is unknown. Above the saprolite layer, proglacial lacustrine sediments, 8 to 12 m thick, were deposited, but no gold grains were found (Shilts and Smith 1988). The Rivière du Moulin erodes mainly Pleistocene cover including glacial and alluvial sediments. The till cover (Fig. 1) is composed of three units, from the oldest to the most recent (Shilts and Smith 1988; Shilts and Caron 2018): 1) the Johnville till that was deposited by a southeast flowing glacier and contains saprolite clasts. One gold grain was reported in this formation; 2) the Chaudière till was deposited from a glacier flowing toward the southwest; 3) the Lennoxville till, associated with the last major glacial episode, was deposited by a glacier flowing in a southeasterly direction. No gold grains were reported in the Chaudière and Lennoxville tills (Shilts and Smith 1988). Several gold placers, such as the McArthur-Coupal placer in the Ruisseau des Meules, (Fig. 1) and placers in the Rivière Gilbert to the northeast (Shilts and Smith 1986) are near Rivière du Moulin area (Fig. 1). These placers are characterized by beds and channels of gold-bearing gravel adjacent to fluvial and glacial sedimentary clays. The Ruisseau des Meules is a direct tributary of the Rivière du Moulin, near the end of the transect, and gold mineralized veins are located near the placer (Fig. 1).

The stream flows from south to north and drains mainly sedimentary particles ranging from coarse pebbles to clays (Fig. 1). The river was sampled over 9 km, from the Lac Volet to Rivière Chaudière at Beauceville. The river was selected because of limited anthropogenic disturbances such as bridges, and a limited number of tributaries, which prevents contamination by exotic gold grains (Fig. 1). In this section, the river has an average width of 5.0 m and an average slope of 0.7 degrees, which indicates a low annual flow with two peaks of higher flow rate during snowmelt and during the fall. However, past glacial movements were in the opposite direction of the more recent river flow, which complicates the interpretation of gold grain shape changes during transport (Fig. 1).

Gold grain selection

Gold grains were sampled in the stream bedload using a prospecting pan for the larger visible particles, and by mineral processing for smaller particles (Fig. 1). The larger grains were mainly collected at the beginning of the transect, while the smaller particles were collected towards the end of the transect (Fig. 1). The first sampling point corresponds to the first grain found in the river and will be taken as the origin of the transect because the source of gold particles is unknown (Fig. 1).

Six large gold grains (185 to 909 µm) collected from 5 locations with prospecting pan were analyzed with µCT and are the whole of the samples (Fig. 1). Eleven gold grains from 7 locations were separated from the alluvial matrix (~15 kg per sample) by commercial mineral processing at Overburden Drilling Management Limited (ODM). ODM separates the gold grains using a shaking table and hand-picking, which have a moderate impact on the change of gold grains shape. According to ODM morphology report, which is considered qualitative, all gold grains in each sample have similar physical characteristics such that they are representative of the sample. For each sample, the largest and most visible gold grain was selected for analysis. A set of 7 small gold grains (42 to 83 µm) were selected along the stream to be analyzed with SEM photogrammetry and 6 large gold grains was collected to be analyzed with µCT (Fig. 1). For each sampling point, one gold grain was analyzed with SEM photogrammetry or µCT, except for (i) the samples at 0.00 and 6.63 km, where two grains of different sizes were analyzed with both methods and (ii) the sample at 2.45 km, where two grains collected with the prospecting pan were analyzed with µCT. In summary, 13 grains were reconstructed in 3D, which is limited number of measurements compared to classical 2D studies that analyze a hundred or thousands of gold grains (Knight et al. 1999; Youngson and Craw 1999; Townley et al. 2003).

Morphometric quantification of alluvial gold grains from the Rivière du Moulin

The 13 gold grains are labelled according to their distance from the first sample. Seven grains were analyzed by SEM photogrammetry with grain sizes varying between 42.1 µm and 83.5 µm for the long axis (Fig. 2). The volume of these particles ranges from 2,013 μm^3 to 82,840 μm^3 (Fig. 2). The texture of gold grains is variable and some grains have a film of carbon-rich material on the surface, whereas the others are free of carbon matter with a smooth or striated surface (Fig. 2). Six grains were analyzed with µCT (Fig. 2). Their long axis varies between 184.8 µm and 909.4 µm, and the volume between 237,778

μm³ and 74,513,080 μm³ (Fig. 2). The surface texture is not represented with this method, but cavities in the larger grains are preserved (Fig. 2).

The gold grains geometry in the Rivière du Moulin is diverse (Fig. 2): 1) one grain reconstructed using SEM photogrammetry (5.95 km) is spheric and considered to be a particle of simple geometry. One μCT gold grain (2.45 km) is an elongated block and is also considered as a having simple geometry; 2) three grains (0.00, 7.05, and 7.60 km) have a complex geometry. The grain at 7.60 km is attached to the carbon tape, causing erroneous extra volume for the grain, whereas the grains at 0.00 and 7.05 km have an irregular shape but a small surface was in contact with the carbon tape; 3) three SEM photogrammetry grains (6.63, 8.63, and 9.01 km) and five μCT grains (0.00, 1.97, 2.45, 4.46, and 6.63 km) have flat geometry. These particles were attached to a face in the direction of the longest axis such that the contact surface with the carbon tape is large considering the error in volume and short axis. The grain at 1.97 km is the largest particle and has an elongated block shape (Fig. 2). The grain at 4.46 km is flat and complex with branched-like geometry (Fig. 2). Gold grains reconstructed with SEM photogrammetry show surface texture partly covered by a film of carbon-rich material (Fig. 2). In addition to visual descriptions, shape parameter and descriptor estimates were measured and computed by SEM photogrammetry and μCT to quantify grains morphology in order to estimate the morphological change during fluvial transport (Table 2).

Discussion

3D quantification, shape parameters, and shape descriptors

The optimal use of μCT and SEM photogrammetry depends on grain size and inherent resolution of both methods. Each method has advantages and pitfalls. On one hand, the μCT provides a complete reconstruction of the grain based on attenuation images but the resolution is not optimal for small gold grains (Masson et al. 2020). The 3D reconstruction allows accurate estimation of the axial lengths, surface area and volume of the particle and is independent of grain geometry. On the other hand, SEM photogrammetry yields detailed surface texture of the grain but the face in contact with the conductive tape is not reconstructed, which causes error in the model (Masson et al. 2020). This method is effective for particles with simple geometry, but requires a careful installation of complex and flat particles on the support. Thus, it is recommended to limit the surface area of the grain in contact with the carbon tape to

avoid error in volume and shape parameters (Masson et al. 2020). The two methods enable quantification of a wide range of gold grain sizes and estimation of shape parameters in order to quantify their morphology.

Intrinsic shape parameters, such as the long axis (*L*), intermediate axis (*I*), short axis (*S*), surface area (*A*), volume (*V*), volume of the convex hull (*Vch*), radius of the largest inscribed sphere (*Ri*), and radius of the smallest circumscribed sphere (*Rc*) are measured directly on the particle (Table 2). The volume is an essential parameter because it yields the effective size of the particle in 3D. The long axis is not usually correlated with the volume of the largest particles (Table 2). The volume therefore independent of the long axis that is usually used to estimate a particle size. The volume is also more robust than the surface area, because it is less constrained to digitalization during the production of 3D models. The 3D surface area is another key parameter, but its measure depends on the texture details resulting from the 3D reconstruction (Masson et al. 2020). Thus, the use of this parameter is challenging in order to quantify the morphology of a grain, but they provide a quantification of roundness, which until now has been estimated qualitatively.

Shape descriptors yield quantitative values of the grain morphology and can be polyvalent to compute more than one descriptor (Table 1). For example, the *degree of true sphericity* (Ψ) is correlated with the *roundness index* (*Xs*) (Hayakawa and Oguchi 2005), and was used in this study to estimate roundness. The *sphericity index* (*I.sph*) is correlated with the *Wentworth flatness index* and provides a flatness index, useful to estimate flatness with volumetric parameters (Table 1). The *sphericity index* has the advantage to be based on the volume and the short axis, which are accurately measured with µCT. The *ellipticity shape descriptor* (*Esd)* and the *Es index* (*Es)* compare the particle with an ellipsoid using the volume and surface area, respectively (Table. 1). By visual observations of the gold grains, the *ellipticity shape descriptor* is more robust to quantify the ellipticity than the *Es index*. In this study, the µCT grain at 4.46 km (Table 2) is considered elliptic by the *Es index* (*Es* = 0.95), but is not considered elliptic using the *ellipticity shape descriptor* (*Esd* = 0.51) and visual observation confirms the non-elliptic nature of this grain (Fig. 3). Thus, the *ellipticity shape descriptor* is used in this study to estimate ellipticity, whereas the *Es index*, which is related to the *roundness index* (*Ir*), is used to estimate roundness. The computation of several shape descriptors

(using different shape parameters) is recommended to completely characterize sedimentary and gold particles.

Change of gold grains shape along the Rivière du Moulin

In fluvial environments, the decrease in gold particles size with increasing distance of transport is documented by the change of the particle long axis (Knight et al. 1999; Craw et al. 2013). The 3D reconstruction yields the volume measurement of gold grains and yields the particle size without the long axis measurement. The volume of gold grains depends on the geometry of the particle and the method of analysis. The μCT yields a complete reconstruction and an accurate volume measurement of the gold particle, whereas the SEM photogrammetry yields a partial model and a less accurate volume measurement. However, the analytical errors on particle volume measurements remain small between the two methods (Masson et al., 2020). The long axis of a flat particle can be significant, while the volume remains constant, which can lead to an apparent variation. In this study, the gold grains analyzed with the μCT were located at the beginning of the transect (0.00 to 6.63 km), whereas gold grains analyzed with the SEM photogrammetry were located mostly at the end (5.95 to 9.01 km) of the transect (Fig. 1). In the Rivière du Moulin, the 13 gold grains show a decrease of volume with increasing distance of transport (Table 2), which is also true for the surface area. This trend is not observed for the gold grains analyzed by μCT, while those analyzed by SEM photogrammetry show a decrease of volume and surface area at the end of the stream (Table 2).

In this study, we assumed that the morphological change during transport does not depend on the analytical method used for the 3D reconstruction of gold particles. This simplification allows to describe changes by linear regressions computed from the shape descriptor values of the 13 gold grains with respect to distance (Fig. 3). A linear regression (95% of confidence) is computed to investigate the morphological changes (Fig. 3). The flatness (*FI, CSF, I.sph*), sphericity (*Hr*, *Ψ.op*, *Ψ.is)*, two roundness (*Ψ, Xs*), convexity (*Co*, *CE*) and ellipticity (*CE*, *Esd*) shape descriptors do not change significantly along the Rivière du Moulin (Fig. 3A-J). These shape descriptors yield a coefficient of determination (R^2) and a slope close to 0, which indicate a large dispersion of values about the regression line and no significant change along the river (Fig. 3A-J). The values of the flatness indices show the gold grains in the Rivière du Moulin are moderately to highly flat (Fig. 3A-C), which is typical of the fluvial environments

(Youngson and Craw 1999). The *Wentworth flatness index* (*FI*) and *sphericity index* (*I.sph*) increase along the river, amplified by the large range of values for these descriptors, between 0 and +∞ (Fig. 3A-B). These two descriptors are affected by gold grains values of $FI > 4$ ad $I.sph > 15$, such that these two descriptors do not show changes of flatness with the distance (Fig. 3A-B). The *Corey shape factor* (*CSF*) changes between 0 and 1, and confirms that the flatness does not vary with distance of transport (Fig. 3C), which is counter-intuitive with the results of other studies in the fluvial domain (Hérail et al. 1990; Knight et al. 1999; Youngson and Craw 1999). Gold grains with a flat geometry can have a large part in contact with the carbon tape, which leads to significant differences between SEM photogrammetry and µCT (> 19%) for the short axis, radius of the largest inscribed sphere, volume of the convex hull and volume values as well as the shape descriptors computed from these parameters (Masson et al. 2020). Thus, the flatness shape descriptors can lead to the flatness values variations in the transect and show independence of flattening with the distance of transport (Fig. 3A-C). The flatness descriptors can be slightly overestimated if the grain is analyzed with the SEM photogrammetry and the orientation of the grain and its placement are essential to achieve accurate measurements using SEM photogrammetry (Masson et al. 2020). The *Hofmann shape entropy* (*Hr*) indicates high grain sphericity, whereas the *operational sphericity* (*Ψ.op*) and *inscribed sphericity* (*Ψ.is*) indicate moderate sphericity of gold grains, which is confirmed by visual observations (Fig. 3D-F). The *degree of true sphericity* (*Ψ*) and *roundness index* (*Xs*) show moderate values of the roundness for the gold particles (Fig. 3G-H). The *convexity index* (*Co*) and the *convexity and ellipticity shape descriptor* (*CE*) do not change with distance of transport, but the slopes of regression lines (R^2) are higher than values of flatness (*FI, CSF, I.sph*), sphericity (*Hr*, *Ψ.op*, *Ψ.is)*, and roundness (*Ψ, Xs*) shape descriptors (Fig. 3I-J). These two descriptors (*Co*, *CE*) indicate high to moderate compactness and ellipticity of gold particles (Fig. 3I-J). The ellipticity shape descriptors (*Esd)* show a slight decrease of ellipticity along the Rivière du Moulin (Fig. 3K). The *ellipticity shape descriptor* (*Esd)* decreases from 0.80 to 0.60, with a $R^2 = 0.231$ (Fig. 3K). This descriptor indicates a possible slight decrease from high to moderate ellipticity with distance of transport, but the R^2 is not significant (Fig. 3K).

Two roundness indices (*Ir*, *Es*) show a significant increase of roundness along the Rivière du Moulin (Fig. 3L-M). The *roundness index* (*Ir*) decreases from 1.4 to 1 over 9 km, with significant $R^2 = 0.339$ (Fig. 3L). The *Es index* (*Es*) increases from 0.7 to 1 over 9 km, with significant $R^2 = 0.498$ (Fig. 3M).

These two descriptors (*Es*, *Ir*) show a decrease from moderately to highly rounded gold particles with the increase of the distance of transport (Fig. 3L-M). In fluvial domains, the change in gold particle shape is characterized by an increase of flatness and roundness (Giusti 1986; Hérail et al. 1990; Knight et al. 1999; Youngson and Craw 1999; Townley et al. 2003). The change of roundness increases rapidly during the first kilometers of the river and remains unchanged after 5 km (Knight et al. 1999). In the Rivière du Moulin, the roundness increases significantly with distance of transport, but the flatness does not show a significant change (Fig. 3A-C). These two quantitative shape descriptors applied on a small amount of grains shows increase of roundness on a stream of short distance. Finally, analysis of additional gold grains in 3D is needed to confirm these changes, especially for the flatness indices, the decrease of ellipticity (Fig. 3K) and the increase of roundness (Fig. 3L-M) with increasing distance.

Change in shape of gold grains in relation to Quaternary history

The shape descriptors can be affected by gold grains coming from multiple sources (Fig. 1). In a context where the source is unknown and glacial transport is opposite to river flow, the shape of the first gold grains collected upstream is used as a reference, but the possibility of multiple sources brings challenges to the interpretation of shape evolution (Fig. 1). The changes in morphology can be affected by exotic gold grains coming from other tributaries or by a later release of grains downstream that will not reflect the change in shape related to fluviatile transport of the Rivière du Moulin. Four possible sources for the origin of these particles should be considered: 1) gold-bearing veins in the surrounding area, but the river does not erode any known source; 2) gold-bearing saprolite beneath the till cover (Shilts and Smith 1988; Shilts and Caron 2018), but no evidence of erosion of the saprolite by the river is observed; 3) gold grains from the till cover deposited by the generally southward flow of ancient glaciers (Fig. 1). The low number of gold grains in the Lennoxville till (n=0), the Chaudière till (n=0) and in the underlying Johnville till (n=1) indicate the tills have a very low gold content; 4) gold placers in the Ruisseau des Meules, which is a main tributary at the end of the Rivière du Moulin transect (Fig. 1). The contribution of the Ruisseau des Meules placer may explain the high values for roundness descriptors (*Es* and *Ir*) for the last two grains of this transect (Fig. 3L-M), but cannot be the source of the gold grains collected upstream.

Glacial and fluvial transports occurred in opposite directions (Fig. 1), which complicates the interpretation of morphological changes. It seems very difficult to separate changes in shape descriptors from these two events without a detailed study of gold grains that would be sourced from the till deposits. Gold grains could be deformed in the till and then in the alluvium. Fluvial transport can also obliterate traces of previous glacial transport by erasing surface traces, which can make the identification of the source complex. Solution-precipitation in saprolite, preglacial mechanical erosion and glacial redistribution are factors that may have modified the shape of gold grains (Shilts and Smith 1988), assuming the gold grains in the Rivière du Moulin were eroded from underlying till. These processes complicate the identification of the source through changes of shape descriptor values with transport. The characterization of gold grain morphology from known occurrences (Fig. 1), as well as the analysis of gold and other indicator mineral chemical composition would likely be required to constrain the source of gold of this complex geological setting.

Evaluation of morphometric approaches and future work for mineral exploration

There are several methods to estimate the morphology of gold grains and each method has benefits for application to mineral exploration in the fluvial environment. The 2D methods are faster and enable to characterize the flatness and sphericity of hundreds and thousands of gold grains using length measurements (Townley et al. 2003; Crawford 2007; Crawford and Mortensen 2009; Wrighton 2013; Barrios et al. 2015). However, precision of measurements is dependent on the operator (Crawford and Mortensen 2009). The PCA function, the method of Crawford and Mortensen. (2009) using ImageJ plug-in, and a MeshLab software (Cignoni et al. 2008) were tested on gold grains from the Rivière du Moulin and results are compared with particle length measurements from the 3D minimal bounding box (Fig 4A and 4D). The PCA function is applied on 3D model (Fig. 4A and 4D). The grain is oriented according to the moments of inertia in order to estimate the long axis first and then the intermediate and short axis (Fig. 4A and 4D). For the ImageJ and MeshLab methods, the 2D projection (#1) was used to measure the long axis and a secondary (*I* or *S*) axis (Fig. 4B-C and 4E-F). After a rotation of 90 degrees of the projection (#1), a second projection (#2) was used to measure the third (*I* or *S*) axis (Fig. 4B-C and 4E-F). The first grain (Fig. 4A-C) shows values of the long, intermediate and short axes similar to the minimal bounding box measurements on the 3D model, the PCA (Fig. 4A), the ImageJ (Fig. 4B), and the

MeshLab (Fig. 4C) measurements. However, the second grain (Fig. 4D-F) shows a larger difference between the minimal bounding box and the PCA measurements (Δ = 67.6 μm for the long axis) (Fig. 4D), the ImageJ measurements (Δ = 73.8 μm for the intermediate axis) (Fig. 4E), and the MeshLab measurements (Δ = 61.3 μm for the long axis) (Fig. 4F), which will lead to differences in computed shape descriptors.

The dimensions of the 13 gold grains from the Rivière du Moulin were measured using the 4 methods (Table 3). The comparison is based on the estimation of the minimal bounding box from μCT and SEM photogrammetry (Table 2). Several shape descriptors that use particle size are compared to discuss the impact of measurement variations on 2D flatness and sphericity shape descriptors (Table 3). The measurement and shape descriptor differences between the minimal bounding box and the MeshLab methods are important (mean value up to 70%) and highlights the importance the choice of software to estimate dimension values (Table 3). The measurements using ImageJ show a mean difference of 2 to 8% on the dimension values, and a maximum of 9% on the shape descriptors computed from the dimensions, such that the measurements are nearly similar between the two methods (Table 3). However, there is uncertainty on the measurement of the axes with the ImageJ and MeshLab methods because two projections are needed to measure the triaxial lengths (Fig. 4). Two projections measure the same axis, but the values of the two axes can be different (Fig. 4E-F). Thus, the selection of the long axis value (Fig. 4E-F) depends on the operator, which will impact the value of the shape descriptor. The two 3D methods yield values for each axis, but the measurement from the minimal bounding box is time-consuming (Fig. 4A and 4D). A faster alternative is to apply the PCA function to the 3D model (Fig. 4A and 4D). This method shows few differences (maximum mean value = 6%) with the minimal bounding box measurements (Table 3). The PCA is the fastest of the 4 methods for particle size estimation and could be benefit for 2D and 3D quantification.

The use of image analysis is essential to estimate the particle dimensions in order to limit the error on the short axis (Table 3). The position of the gold grain on the support is a key factor for 2D and 3D measurements (Crawford and Mortensen 2009; Masson et al. 2020). Using optical and SEM methods, the particle orientation has high impact on 2D and 3D measurements, but the μCT method does not depend on the orientation and yields an accurate measurement of length, volume and surface area (Masson et al.

2020). However, μCT is more expensive, less accessible, and the processing time is greater than SEM photogrammetry and other optical methods (Masson et al. 2020). SEM is a polyvalent tool to quantify the morphology of gold grains in 2D and 3D (with photogrammetry). This method is relatively fast and enables the surface texture (marks, striations, inclusions) of gold particles to be studied, but remains time-consuming for the analysis of several thousand grains. The 3D methods are supported by image analysis to estimate shape parameters (Masson et al., 2020). For our case study, the contribution of the 3D method is justified since the number of gold grains collected in the river was small. The 3D method yields new shape parameters (surface area, volume and volume of the convex hull) that enable the computing of additional shape descriptors (roundness, sphericity, and ellipticity) previously could only be estimated qualitatively. These descriptors completely characterize the gold particle shapes and can be useful to identify morphological changes during fluvial transport.

Conclusion

Since the 1970s, the methods for estimating the shape of gold grains have evolved from 2D qualitative to semi-quantitative analysis. In this study, we use X-ray microtomography and SEM photogrammetry to reconstruct the morphology of gold grains in 3D and apply this to describe alluvial particles shape along the distance of transport. Shape parameters and 3D shape descriptors are computed to estimate the change of gold grains morphology according to the distance of transport.

The flatness (*CSF, FI, I.sph*), sphericity (*Hr*, *Ψ.op*, *Ψ.is*), roundness (*Ψ*, *Xs, Ir, Es*), convexity (*Co*, *CE*), and ellipticity (*CE*, *Esd*) shape descriptors estimated on 13 gold grains along the 9 km of the Rivière du Moulin show: 1) a decrease in volume relative to a decrease in particle size with distance of transport; 2) non-significant changes of flatness (moderately to highly flat), sphericity (moderately spheric), two roundness (moderately rounded), and convexity (compact) shape descriptors of gold grains shape along the river; 3) a slight decrease of ellipticity (*Esd*), from highly to moderately elliptic particles; 4) an increase of roundness (*Ir*, *Es*), from moderately to highly rounded gold particles. Some factors limit the insights that can be gained from the shape change of gold grains, including (i) the unknown source, (ii) the complex transportation environment, (iii) the limited number of gold grains analyzed, and (iv) the short distance of transport along the river. The application of these shape descriptors in other rivers with a

known source should be attempted to estimate an accurate shape-distance of transport relationship, which is efficient to trace the particle source in mineral exploration.

Comparison of the 2D and 3D methods shows that both approaches are useful. This study shows the benefits using image analysis to measure particle dimensions accurately and to automate the method by reducing operator bias. We suggest to use 2D methods for a fast study on a large number of gold grains, whereas 3D methods should be favored for a more detailed study on a limited number of gold grains. The 3D approach enables the estimation of the volume which characterize the particle completely, in contrast to the long axis, which is commonly measured on a 2D section. Shape descriptors based on 2D methods are useful to quickly estimate flatness and sphericity descriptors for a large number of gold grains whereas 3D methods yield additional shape parameters (radius of the largest inscribed sphere, radius of the smallest circumscribed sphere, surface area, volume of the convex hull, and volume) in order to quantify additional shape descriptors (roundness, sphericity, convexity, and ellipticity) that can be used in case studies of morphological changes during fluvial transport.

Acknowledgments

We would like to thank Émilie Bédard and Roman Hanes for their help in the field and the sampling. We thank Overburden Drilling Management Limited (ODM ldt) for the mineral processing of gold grains as well as Stéphane Gagnon for the data-acquisition analyses with the SEM at Université Laval and Rui Tahara for the data-acquisition analyses with the Xradia 520 Versa (XRM) at McGill University. We thank Dave Craw, James K Mortensen, and Robert J Chapman for their useful advices to improve our manuscript as well as Isabelle McMartin, Pierre Francus, and Eric Pirard for their helpful comments.

Funding

The research presented in this paper was funded by the Natural Sciences and Engineering Research Council of Canada (NSERC) in partnership with Agnico Eagle Mines Ltd and the Ministère de l'Énergie et des Ressources Naturelles du Québec (MERN).

References

Alshibli, K.A., Druckrey, A.M., Al-Raoush, R.I., Weiskittel, T. & Lavrik, N.V. 2014. Quantifying morphology of sands using 3D imaging. *Journal of Materials in Civil Engineering*, **27**, 04014275-04014271-04014275-04014210.

Aschenbrenner, B.C. 1956. A new method of expressing particle sphericity. *Journal of Sedimentary Research*, **26**, 15-31.

Barrios, S., Merinero, R., Lozano, R. & Orea, I. 2015. Morphogenesis and grain size variation of alluvial gold recovered in auriferous sediments of the Tormes Basin (Iberian Peninsula) using a simple correspondence analysis. *Mineralogy and Petrology*, **109**, 679-691.

Chapman, R.J. & Mortensen, J.K. 2006. Application of microchemical characterization of placer gold grains to exploration for epithermal gold mineralization in regions of poor exposure. *Journal of Geochemical Exploration*, **91**, 1-26.

Chapman, R.J. & Mortensen, J.K. 2016. Characterization of Gold Mineralization in the Northern Cariboo Gold District, British Columbia, Canada, Through Integration of Compositional Studies of Lode and Detrital Gold with Historical Placer Production: A Template for Evaluation of Orogenic Gold Districts. *Economic Geology*, **111**, 1321-1345.

Cignoni, P., Callieri, M., Corsini, M., Dellepiane, M., Ganovelli, F. & Ranzuglia, G. 2008. Meshlab: an open-source mesh processing tool. *Eurographics Italian Chapter Conference*, 129-136.

Corey, A. 1949. Influence of shape on the fall velocity of sand grains: Colorado A & M College (now Colorado State University), Fort Collins, unpub. *Master's thesis*, 102.

Craw, D., & Lilly, K. 2016. Gold nugget morphology and geochemical environments of nugget formation, southern New Zealand. *Ore Geology Reviews*, **79**, 301-315.

Craw, D., Hesson, M. & Kerr, G. 2017. Morphological evolution of gold nuggets in proximal sedimentary environments, southern New Zealand. *Ore Geology Reviews*, **80**, 784-799.

Crawford, E.C. 2007. Klondike placer gold: New tools for examining morphology, composition and crystallinity. M.Sc. thesis, University of British Columbia.

Crawford, E.C. & Mortensen, J.K. 2009. An ImageJ plugin for the rapid morphological characterization of separated particles and an initial application to placer gold analysis. *Computers & Geosciences*, **35**, 347-359.

Dilabio, R. 1991. Classification and interpretation of the shapes and surface textures of gold grains from till. *Gisements alluviaux d'or (Alluvial Gold Placers/Yacimientos aluviales de oro)*. ORSTOM Paris, 297-313.

Eyles, N. 1989. Post-depositional nugget accretion in Cenozoic placer gold deposits, Cariboo mining district, British Columbia (93 A, B, G, H). *BC Ministry of Energy, Mines and Petroleum Resources*, 147-169.

Folk. R.L. 1955. Student operator error in determination of roundness, sphericity, and grain size: *Journal of Sedimentary Petrology*, **25**.

Fonseca, J., O'sullivan, C., Coop, M.R. & Lee, P. 2012. Non-invasive characterization of particle morphology of natural sands. *Soils and Foundations*, **52**, 712-722.

Giusti, L. 1986. The morphology, mineralogy, and behavior of " fine-grained" gold from placer deposits of Alberta: sampling and implications for mineral exploration. *Canadian Journal of Earth Sciences*, **23**, 1662-1672.

Hallbauer, D. & Utter, T. 1977. Geochemical and morphological characteristics of gold particles from recent river deposits and the fossil placers of the Witwatersrand. *Mineralium Deposita*, **12**, 293-306.

Hayakawa, Y. & Oguchi, T. 2005. Evaluation of gravel sphericity and roundness based on surface-area measurement with a laser scanner. *Computers & Geosciences*, **31**, 735-741.

Hébert, Y. 2001. Étude structurale du lineament Magador, Région de Beauceville, Projet Magador. *In*: (FEMECA), L.F.D.E.M.R.D.L.E.T.C.I.R.-A. (ed.). Ministère des Ministère de l'Énergie et des Ressources naturelles.

Hérail, G., Fornari, M. & Rouhier, M. 1989. Geomorphological control of gold distribution and gold particle evolution in glacial and fluvioglacial placers of the Ancocala-Ananea basin-Southeastern Andes of Peru. *Geomorphology*, **2**, 369-383.

Hérail, G., Fornari, M., Viscarra, G. & Miranda, V. 1990. Morphological and chemical evolution of gold grains during the formation of a polygenic fluviatile placer: the Mio-Pleistocene Tipuani placer example (Andes, Bolivia). *Chronique de la recherche miniere*, 41-49.

Hofmann, H. 1994. Grain-shaped indices and isometric graphs. *Journal of Sedimentary Research*, **64**, 916-920.

Janke, N. 1966. Effect of shape upon the settling vellocity of regular convex geometric particles: *Journal of Sedimentary Petrology*, **36**, 370-376.

Kerr, G., Falconer, D., Reith, F. & Craw, D. 2017. Transport-related mylonitic ductile deformation and shape change of alluvial gold, southern New Zealand. *Sedimentary Geology*, **361**, 52-63.

Knight, J., Morison, S. & Mortensen, J. 1999. The relationship between placer gold particle shape, rimming, and distance of fluvial transport as exemplified by gold from the Klondike District, Yukon Territory, Canada. *Economic Geology*, **94**, 635-648.

Krumbein, W.C. 1941. Measurement and geological significance of shape and roundness of sedimentary particles: *Journal of Sedimentary Petrology*, **11**.

Le Roux, J. 1997. Comparison of sphericity indices as related to the hydraulic equivalence of settling grains. *Journal of Sedimentary Research*, **67**, 527-530.

Loen, J.S. 1995. Use of placer gold characteristics to locate bedrock gold mineralization. *Exploration and Mining Geology*, **4**, 335-339.

Masson, F.-X. 2020. Quantification 3D de la morphologie des grains d'or dans les sédiments meubles. Ph.D. thesis, Université Laval.

Masson, F.-X., Beaudoin, G. & Laurendeau, D. 2020. Quantification of the morphology of gold grains in 3D using X-ray microscopy and SEM photogrammetry. *Journal of Sedimentary Research*, **90**, 286-296, doi: 10.2110/jsr.2020.16.

McClenaghan, M.B. & Cabri, L.J. 2011. Review of gold and platinum group element (PGE) indicator minerals methods for surficial sediment sampling. *Geochemistry: Exploration, Environment, Analysis*, **11**, 251–263.

Minter, W. 1999. Irrefutable detrital origin of Witwatersrand gold and evidence of eolian signatures. *Economic Geology*, **94**, 665-670.

Minter, W., Goedhart, M., Knight, J. & Frimmel, H. 1993. Morphology of Witwatersrand gold grains from the Basal Reef; evidence for their detrital origin. *Economic Geology*, **88**, 237-248.

Nakagawa, M., Santosh, M., Nambiar, C. & Matsubara, C. 2005. Morphology and chemistry of placer gold from Attappadi Valley, southern India. *Gondwana Research*, **8**, 213-222.

Powers, M.C. 1953. A new roundness scale for sedimentary particles. *Journal of Sedimentary Petrology*, **23**, 117-119.

Rasmussen, K., Mortensen, J., Falck, H., Emond, D., Lewis, L. & Weston, L. 2006. Morphological and compositional analysis of placer gold in the South Nahanni River drainage, Northwest Territories. *Yukon Exploration and Geology*, 237-250.

Riley, N.A. 1941. Projection sphericity. *Journal of Sedimentary Petrology*, **11**, 94-97.

Schneider, C.A., Rasband, W.S. & Eliceiri, K.W. 2012. NIH Image to ImageJ: 25 years of image analysis. *Nature methods*, **9**, 671-675.

Shilts, W. & Smith, S. 1986. Stratigraphy of placer gold deposits; overburden drilling in Chaudiere Valley, Quebec. *Geol. Surv. Can. Pap*, **86**, 703-712.

Shilts, W.W. & Smith, S.L. 1988. Glacial geology and overburden drilling in prospecting for buried gold placer deposits, southeastern Quebec. *Prospecting in areas of glaciated terranes: Sherbrooke, Canadian Institute of Mining and Metallurgy*, 141-168.

Shilts, W.W. & Caron, O.J. 2018. Glacial history reflected by geochemically constrained stratigraphic sections in the Chaudière River drainage basin of the Canadian Appalachians. *Quaternary Research*, **91**, 234-249.

Townley, B.K., Hérail, G., Maksaev, V., Palacios, C., de Parseval, P., Sepulveda, F., Orellana, R., Rivas, P. & Ulloa, C. 2003. Gold grain morphology and composition as an exploration tool: application to gold exploration in covered areas. *Geochemistry: Exploration, Environment, Analysis*, **3**, 29-38.

Utter, T. 1979. The morphology and silver content of gold from the Upper Witwatersrand and Ventersdorp Systems of the Klerksdorp gold field, South Africa. *Economic Geology*, **74**, 27-44.

Utter, T. 1980. Rounding of ore particles from the Witwatersrand gold and uranium deposit (South Africa) as an indicator of their detrital origin. *Journal of Sedimentary Petrology*, **50**, 71-76.

Wadell, H. 1932. Volume, shape, and roundness of rock particles. *The Journal of Geology*, **40**, 443-451.

Wadell, H. 1933. Sphericity and roundness of rock particles. *The Journal of Geology*, **41**, 310-331.

Wentworth, C.K. 1922. The shapes of beach pebbles. *US Geol. Surv. Prof. Pap.*, **131-C**, 75-83.

Wierchowiec, J. 2002. Morphology and chemistry of placer gold grains–indicators of the origin of the placers: an example from the East Sudetic Foreland, Poland. *Acta Geologica Polonica*, **52**, 563-576.

Wrighton, T. 2013. Placer gold microchemical characterization and shape analysis applied as an exploration tool in western Yukon. M.Sc. thesis, University of British Columbia.

Yeend, W.E. 1975. Experimental abrasion of detrital gold. *Journal of Research of the US Geological Survey*, **3**, 203-212.

Youngson, J.H. & Craw, D. 1999. Variation in placer style, gold morphology, and gold particle behavior down gravel bed-load rivers; an example from the Shotover/Arrow-Kawarau-Clutha River system, Otago, New Zealand. *Economic Geology*, **94**, 615-633.

Youngson, J.H., Wopereis, P., Kerr, L.C. & Craw, D. 2002. Au-Ag-Hg and Au-Ag alloys in Nokomai and Nevis valley placers, northernSouthland and Central Otago, New Zealand, and their implications for placer-source relationships. *New Zealand Journal of Geology & Geophysics*, **45**, 53-69.

Zingg, T. 1935. *Beitrag zur schotteranalyse*, Schweiz. Mineral. Petrogr. Mitt., 15, 39–140.

Figure Captions

Fig. 1. *Quaternary geological map (based on SIGÉOM data) of the Rivière du Moulin with the location of the samples.*

Fig. 2. *3D reconstructions of the alluvial gold grains collected in the Rivière du Moulin. The grain size is estimated using the long axis (L) and volume (V).*

Fig. 3. *Change of shape descriptors according to distance along the Rivière du Moulin. The regression line equation and the determination coefficient (R^2) are computed for each descriptor.*

Fig. 4. *3D and 2D methods to estimate the dimension of two gold grains.* ***A-C****) First gold grain.* ***D-F****) Second gold grain. The green lines represent the minimal bounding box of the grain. The orange lines represent the axes measured on the 2D projections. Abbreviations: L = long axis, I = intermediate axis, S = short axis.*

Table 1. *Shape descriptors used to quantify the morphology of gold grains.*

Name	Formula	Typical particle shape
Wentworth flatness index, *FI* *Wentworth (1922)*	$\frac{L+I}{2S}$	**2D Flatness index:** 1 (cubic / spherical) to +∞ (flat)
Corey shape factor, *CSF* *Corey (1949)*	$\frac{S}{\sqrt{LI}}$	**2D Flatness index:** 0 (flat) to 1 (cubic / spherical)
Hofmann shape entropy, *Hr* *Hofmann (1994)*	$-\frac{\sum(Pi \,.\, \ln Pi)}{1.0986}$	**2D Settling velocity index / Sphericity index:** 0 (non-spherical or elongate) to 1 (spherical)
Sphericity index, *I.sph* *Alshibli et al (2014)*	$\frac{V}{Vs} = \frac{V}{\frac{4}{3}\pi(\frac{S}{2})^3}$	**3D Flatness / Sphericity index**: 0 (kidney-shaped / discoidal) 1 (perfect sphere) to +∞ (non-spherical / flat)
Es index, *Es* *Hayakawa & Oguchi (2005)*	$\frac{en}{A}$	**3D Ellipsoid / Roundness index**: 0 (non-elliptic / angular with extra surface area) 1 (perfect ellipsoid / rounded) to +∞ (non-elliptic / angular with a loss of surface area)
Roundness index, *Ir* *Alshibli et al (2014)*	$\frac{A}{4\pi(\frac{L+I+S}{6})^2}$	**3D Roundness index**: 0 (angular) 1 (rounded / perfect sphere) to +∞ (rounded, with surface asperities)
Roundness index, *Xs* *Hayakawa & Oguchi (2005)*	$\frac{V}{A\sqrt[3]{L\ I\ S}}$	**3D Roundness index**: 0 (angular) to 0.16 (rounded)
Degree of true sphericity, *Ψ* *Wadell (1932)*	$\frac{s}{A} = \frac{\sqrt[3]{36\pi V^2}}{A}$	**3D Sphericity / Roundness index**: 0 (non-spherical - angular) to 1 (spherical - rounded)
Operational sphericity, *Ψ.op* *Wadell (1933)* *Aschenbrenner (1956)*	$\sqrt[3]{\frac{V}{Vcs}} = \sqrt[3]{\frac{V}{\frac{4}{3}\pi(Rc)^3}}$	**3D Sphericity index**: 0 (non-spherical) to 1 (spherical)
Inscribed sphericity, *Ψ.is* *Masson et al (in prep), based on Riley (1941)*	$\sqrt{\frac{Ri}{Rc}}$	**3D Sphericity index**: 0 (non-spherical) to 1 (spherical)
Convexity index, *Co* *Fonseca et al (2012)*	$\frac{V}{Vch}$	**3D Compactness index**: 0 (non-compact) to 1 (compact)
Ellipticity shape descriptor, Esd *Masson (2020)*	$\frac{V}{Vel} = \frac{V}{\frac{4\pi(L\ I\ S)}{24}}$	**3D Ellipticity index**: 0 (non-elliptic) to 1 (elliptic)
Convexity and ellipticity shape descriptor, *CE* *Masson (2020)*	$\frac{V^2}{Vch\ Vel}$	**3D Compactness / Ellipticity index**: 0 (non-elliptic / non-compact) to 1 (elliptic / compact)

§ Shape parameters: L = long axis; I = intermediate axis; S = short axis; Pi = expression relative to the axial lengths, as example for the long axis, PL = L / (L + I + S); en = surface area of an ellipsoid having the same axial lengths of the particle; A = surface area; Rc = radius of the smallest circumscribed sphere of the convex hull; Ri = radius of the largest inscribed sphere of the convex hull; V = volume; Vcs = volume of the smallest circumscribed sphere; Vs = volume of a sphere with diameter equals to the short axis; Vch = volume of the convex hull; Vel = volume of ellipsoid with the same dimension of the particle.

Table 2. Shape parameters and descriptors estimates of gold grains from the Rivière du Moulin (represented by distance in km).

	SEM photogrammetry							μCT					
Distanc	**0.00**	**5.95**	**6.63**	**7.05**	**7.60**	**8.63**	**9.01**	**0.00**	**1.97**	**2.45**	**2.45**	**4.46**	**6.63**
L (μm)	42.1	67.7	83.5	74.3	62.8	43.1	60.5	516.3	909.4	283.8	893.8	184.8	685.5
I (μm)	33.0	57.1	61.0	58.1	38.4	24.3	27.5	267.6	669.2	175.6	627.2	106.6	313.0
S (μm)	26.8	45.0	25.7	35.9	29.0	6.0	14.3	88.8	290.4	124.9	141.7	45.5	51.5
Ri (μm)	12.7	22.4	12.4	17.1	14.0	3.2	6.9	44.2	145.2	61.8	70.2	22.4	25.6
Rc (μm)	24.1	35.7	43.9	44.3	32.3	21.6	31.5	261.2	473.2	150.7	483.2	94.2	342.9
A (μm^2)	3938	10618	10710	9276	6087	1665	2924	296980	2230496	136911	1653139	39082	363811
en	3595	10021	9840	9718	5672	1777	3222	243584	1187277	114085	953012	37050	348849
V (μm^3)	13456	82840	52042	44202	23460	2013	7129	545080	7451308	292450	2697327	237778	368679
Vch	19639	90365	70405	76479	34427	3148	10727	651113	9784196	361180	4292756	418689	633127
Vcs	5.9E+0	1.9E+0	3.5E+0	3.6E+0	1.4E+0	4.2E+0	1.3E+0	7.5E+0	4.4E+08	1.4E+0	4.7E+08	3.5E+0	1.7E+0
Vs	1.0E+0	4.8E+0	8.9E+0	2.4E+0	1.3E+0	1.1E+0	1.5E+0	3.7E+0	1.3E+07	1.0E+0	1.5E+06	4.9E+0	7.2E+0
Vel	1.9E+0	9.1E+0	6.9E+0	8.1E+0	3.7E+0	3.3E+0	1.2E+0	6.4E+0	9.3E+07	3.3E+0	4.2E+07	4.7E+0	5.8E+0
Fl	1.40	1.39	2.81	1.84	1.74	5.62	3.08	4.41	2.72	1.84	5.37	3.20	9.69
CSF	0.72	0.72	0.36	0.55	0.59	0.19	0.35	0.24	0.37	0.56	0.19	0.32	0.11
Hr	0.98	0.99	0.91	0.96	0.95	0.80	0.85	0.82	0.92	0.95	0.83	0.88	0.72
I.sph	1.34	1.74	5.86	1.82	1.84	17.80	4.66	14.87	5.81	2.87	18.11	4.82	51.55
Es	0.91	0.94	0.92	1.05	0.93	1.07	1.10	0.82	0.53	0.83	0.58	0.95	0.96
Ir	1.09	1.06	1.06	0.94	1.03	0.89	0.80	1.12	1.83	1.15	1.71	0.99	0.95
Xs	0.10	0.14	0.10	0.09	0.09	0.07	0.08	0.08	0.06	0.12	0.04	0.06	0.05
Ψ	0.69	0.87	0.63	0.65	0.65	0.46	0.61	0.50	0.38	0.72	0.26	0.47	0.32
Ψ.op	0.61	0.76	0.53	0.50	0.55	0.36	0.38	0.42	0.55	0.59	0.39	0.41	0.28
Ψ.is	0.73	0.79	0.53	0.62	0.66	0.38	0.47	0.41	0.55	0.64	0.38	0.49	0.27
Co	0.69	0.92	0.74	0.58	0.68	0.64	0.66	0.84	0.76	0.81	0.63	0.57	0.58
Esd	0.69	0.91	0.76	0.54	0.64	0.61	0.57	0.85	0.81	0.90	0.65	0.51	0.64
CE	0.47	0.83	0.56	0.31	0.44	0.39	0.38	0.71	0.61	0.73	0.41	0.29	0.37

Table 3. *Comparison of measurements (in percentage) of the long, intermediate and short axis shape parameters and 2D shape descriptors. The minimum, maximum and mean differences percentages are based on the values of the 13 gold grains from the Rivière du Moulin.*

	Minimum differences (n = 13)			Maximum differences (n = 13)			Mean differences (n = 13)		
Shape parameters and descriptors	**PCA**	**ImageJ**	**MeshLab**	**PCA**	**ImageJ**	**MeshLab**	**PCA**	**ImageJ**	**MeshLab**
Long axis, L (µm)	0 %	0 %	0 %	13 %	5 %	16 %	4 %	2 %	4 %
Intermediate axis, I (µm)	0 %	1 %	0 %	13 %	24 %	11 %	4 %	8 %	4 %
Short axis, S (µm)	2 %	0 %	2 %	15 %	21 %	474 %	6 %	8 %	66 %
Flatness ratio (S/I)	0 %	0 %	12 %	13 %	14 %	513 %	4 %	6 %	70 %
Elongation ratio (I/L)	0 %	0 %	0 %	11 %	24 %	14 %	3 %	8 %	5 %
Equancy ratio (S/L)	0 %	0 %	0 %	14 %	25 %	450 %	5 %	8 %	61 %
Wentworth flatness index	0 %	0 %	3 %	12 %	19 %	83 %	4 %	6 %	26 %
Corey shape factor	0 %	0 %	4 %	14 %	15 %	491 %	4 %	4 %	66 %
Janke form factor	0 %	0 %	1 %	10 %	17 %	433 %	4 %	6 %	57 %
Hofmann Shape Entropy	0 %	0 %	0 %	3 %	6 %	28 %	1 %	1 %	5 %
Krumbein intercept sphericity	0 %	1 %	0 %	6 %	15 %	81 %	3 %	5 %	14 %
Maximum projection sphericity	0 %	0 %	4 %	7 %	10 %	226 %	3 %	3 %	35 %

Shape descriptors: Janke form factor (used as a flatness descriptor) $= \sqrt{\frac{S}{\frac{L^2+I^2+S^2}{3}}}$ *(Janke. 1966); Krumbein intercept sphericity* $= \sqrt[3]{\frac{IS}{L^2}}$ *(Krumbein. 1941); Maximum projection sphericity* $= \sqrt[3]{\frac{S^2}{LI}}$ *(Folk.1955).*

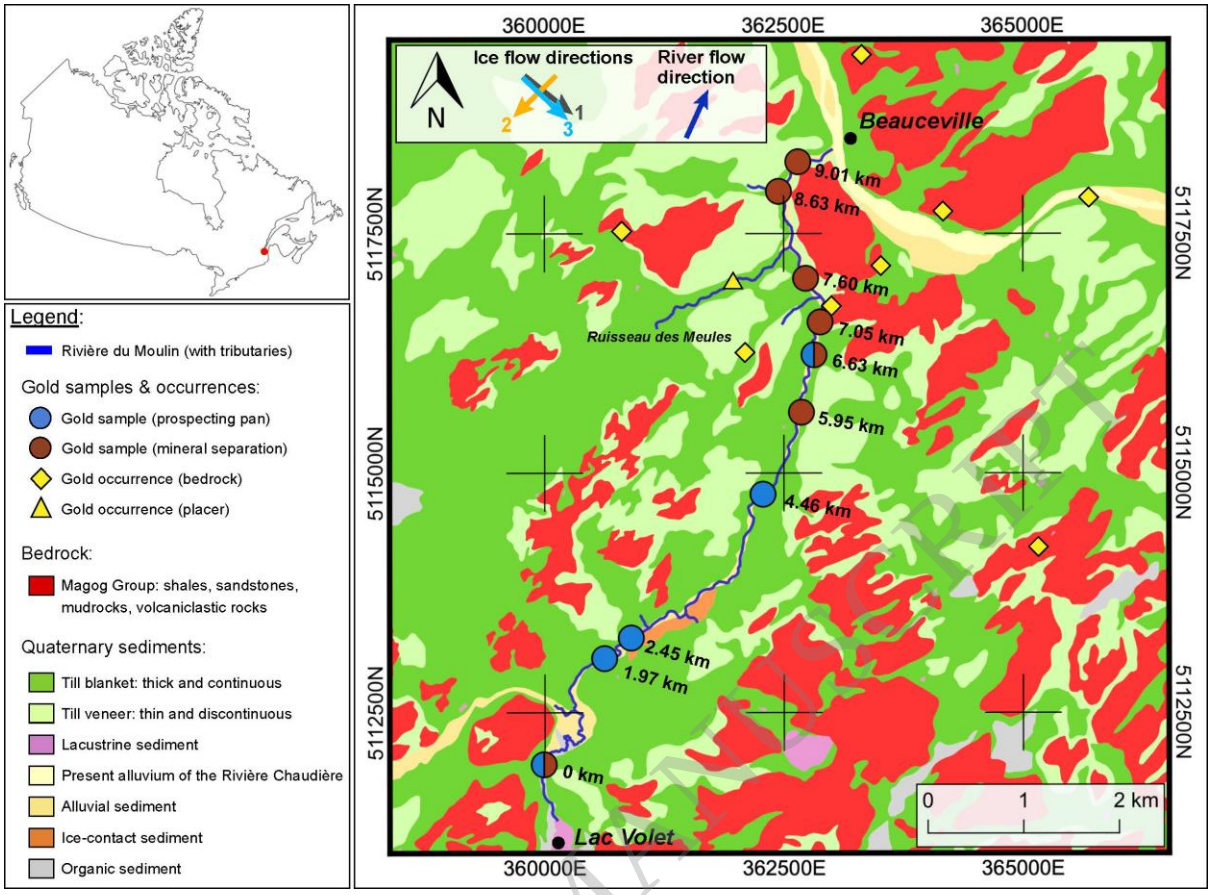

Figure 1

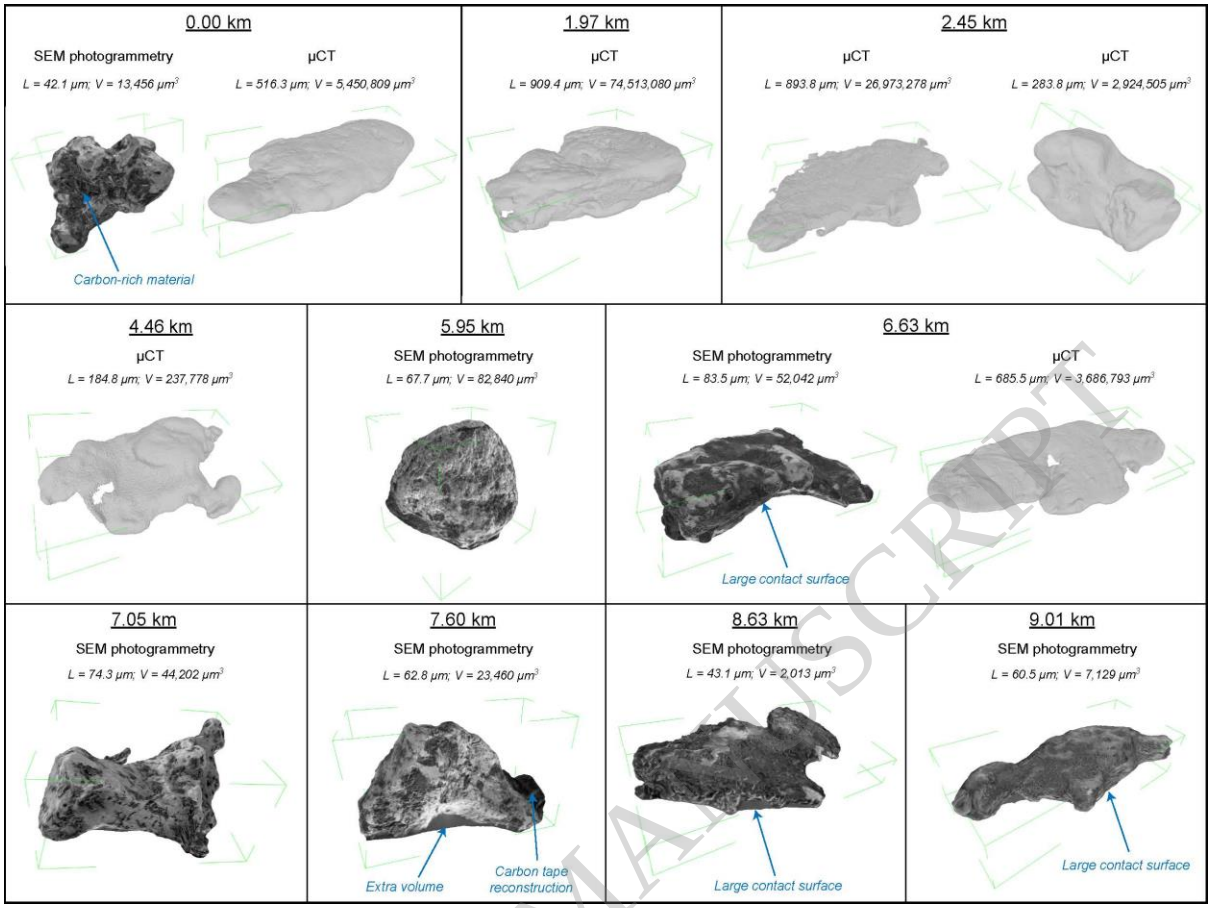

Figure 2

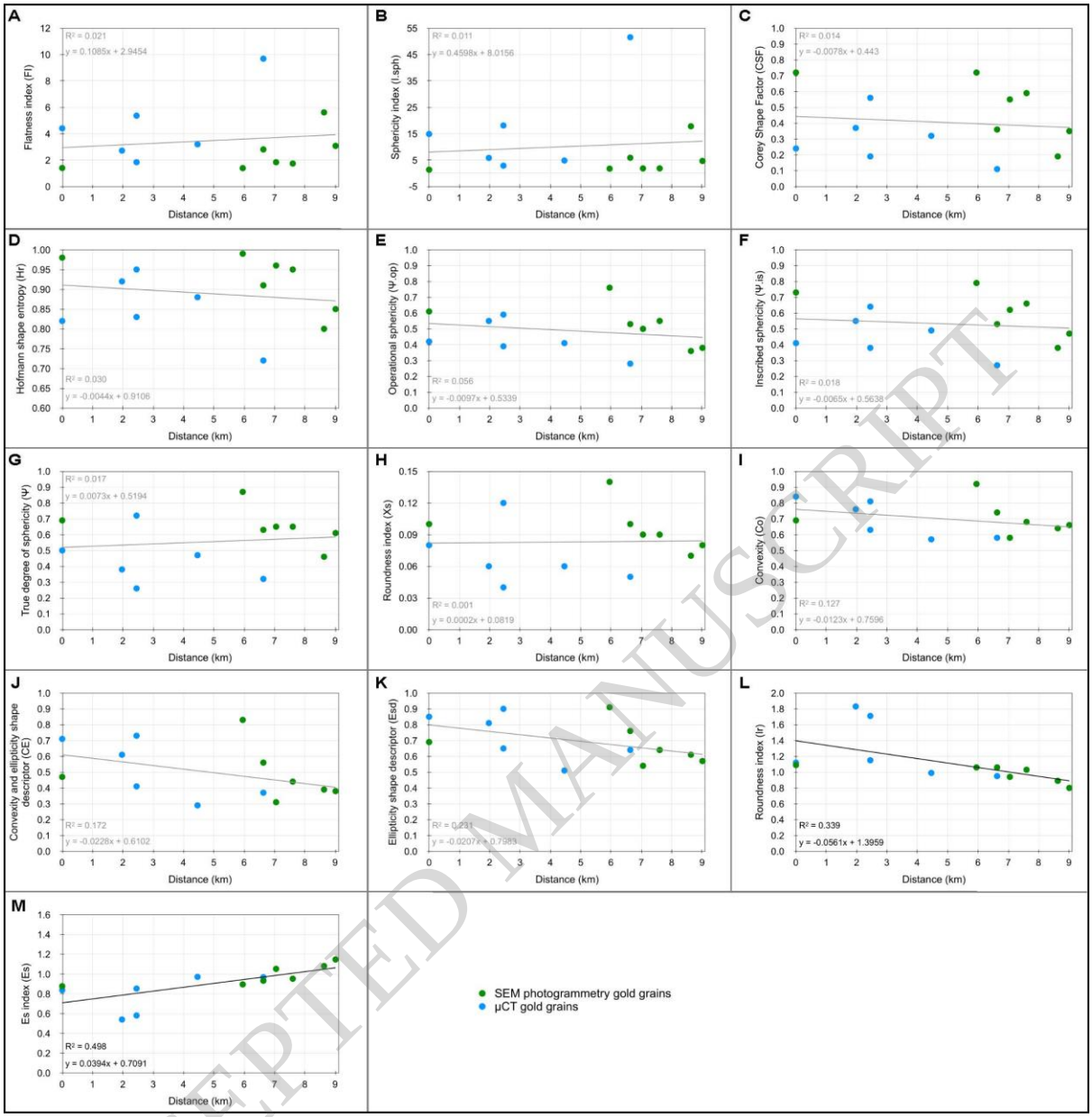

Figure 3

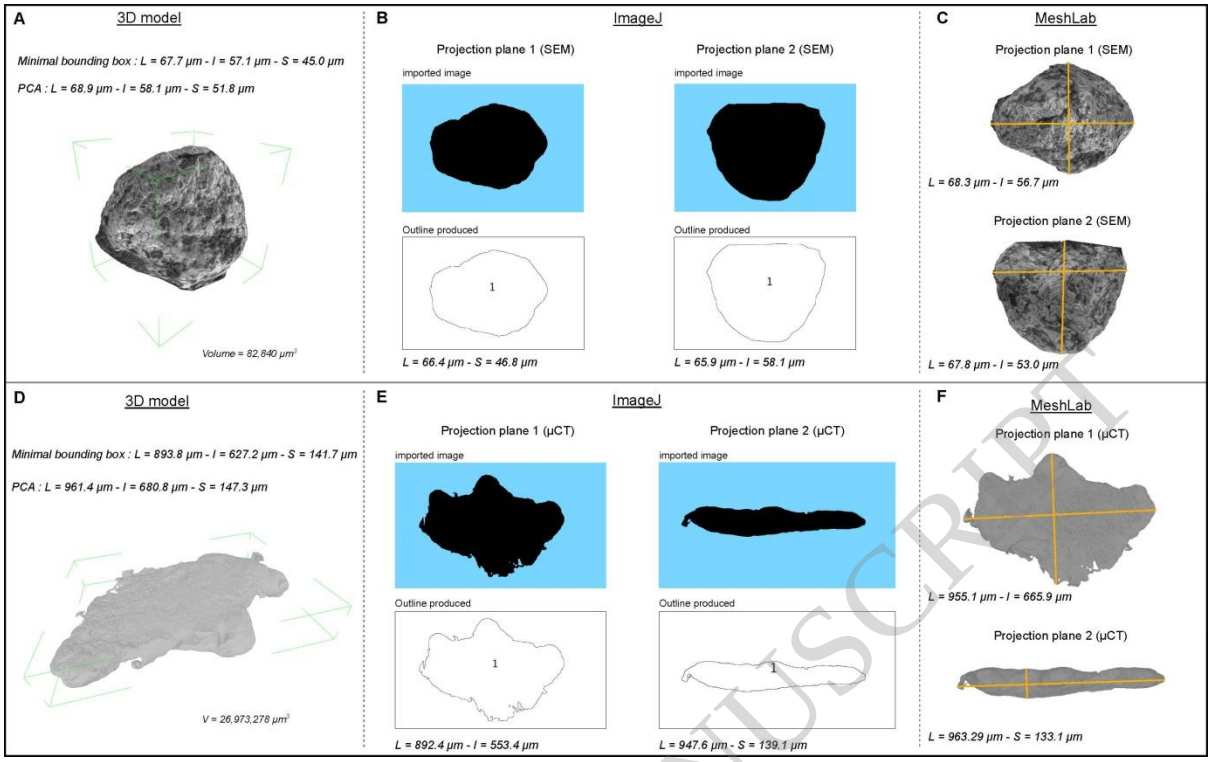

Figure 4